

## FEATURE ARTICLE

## Atom-Resolved Surface Chemistry Using the Scanning Tunneling Microscope

Phaedon Avouris

IBM Research Division, T. J. Watson Research Center, Yorktown Heights, New York 10598  
(Received: October 23, 1989)

Scanning tunneling microscopy (STM) has been proven to be a powerful technique for the study of the electronic topography of surfaces and adsorbed layers. In this article, we demonstrate that STM topographs and atom-resolved tunneling spectra can be used to study the chemical reactivity of surfaces with atomic resolution and relate it to the local electronic structure. In this way, a unique insight into the factors that influence reactivity can be obtained. First, we give an introduction to the technique and the basic concepts on which it is based. We then discuss in some detail three specific examples: (A) the direct imaging of chemical bonds on the Si(100)-(2×1) surface; (B) the site-selective reaction of NH<sub>3</sub> with Si(111)-(7×7); and (C) the interaction of boron with Si(111) and its effect on surface electronic structure, surface reconstruction, and doping effects on chemical reactivity. We close by considering issues relating to the role of the electronic structure of the STM tip and possible future directions in chemical applications of the STM.

## I. Introduction

Atoms at the surface of a solid have fewer neighbors compared with atoms in the bulk material. As a result, surface atoms are characterized by an unsaturated bond-forming capability and are, in general, quite reactive.<sup>1</sup> In this work we will focus on semiconductor solids, particularly silicon. It is common practice to refer to the valence electrons of atoms at semiconductor surfaces that are not involved in bonding as occupying dangling-bond states, and the electrons themselves as dangling bonds. The dangling bonds at the surfaces of semiconductors determine to a large extent the physical (e.g., optical, electrical) and chemical properties of the surfaces of this very important class of solids. In particular, except at high temperatures or in reactions with highly reactive free radicals, the dangling bonds are the "active sites" for surface reactions.<sup>1</sup> Surfaces of solids may have several structurally different active sites. Moreover, all real surfaces have varying numbers of local or extended defects which may also involve broken bonds and which can act as reaction centers. Surface reactions do not only involve atoms of the solid but may also involve adsorbed foreign atoms. Finally, there may be interactions among sites in the sense that reaction at surface site A may influence the reactivity of a neighboring site B. It is clear then that for studying surface chemistry one ideally needs a technique or techniques which will allow one to follow the spatial distribution of the reaction with atomic resolution. Having achieved that goal, one would face the task of explaining the observed reactivity differences at the various surface sites. This can be accomplished by comparing the local electronic structure of the various sites. Thus, we also need tools to study electronic structure with atomic resolution. Until recently, conventional surface electronic structure and topographical techniques were able to provide information averaged over a macroscopic area of the sample, defined by the size of the probe (light, electron, ...) beam used.<sup>2</sup> This area usually encompasses more than 10<sup>11</sup> atomic sites. This picture started changing in 1982 when G. Binnig and H. Rohrer<sup>3</sup> developed the

scanning tunneling microscope—a powerful technique for the study of the electronic topography of surfaces with atomic resolution. Since then, the scanning tunneling microscope has been used successfully to study the structure of clean metal and semiconductor surfaces and adsorbate layers with atomic resolution.<sup>4</sup> These studies have provided important new insights into the nature of surfaces. In this article I will discuss the recent developments in the use of scanning tunneling microscopy (STM) and atom-resolved tunneling spectroscopy to study surface chemistry on an atom-by-atom basis. First, the principles of the technique and of the experiment will be discussed, followed by specific examples from our work on Si surface chemistry. In these studies, STM and atom-resolved tunneling spectroscopy results clearly demonstrate the crucial role of the local electronic structure in determining reactivity.

## II. The STM Experiment

The principle and operation of STM is rather simple. A sharp metal tip, usually made of W or Pt-Ir alloy, is brought very close (e.g., 5–10 Å) to the sample. At this distance the wave functions of the sample and the tip, which are decaying exponentially in the vacuum barrier region, overlap (see Figure 1). If a bias is applied to the sample, an electron tunneling current flows between the two. The direction of electron flow depends on the sign of the bias applied to the sample. For positive sample bias, electrons flow from occupied states of the tip to empty states of the sample. For negative sample bias the direction is reversed. The tip can be moved in three dimensions using three orthogonal piezoelectric translators labeled x, y, and z in Figure 2. The z translator varies the tip–surface distance while the x,y translators scan the tip over the surface. Typically, the tip moves ~10 Å/V applied to a translator. As we will discuss in more detail in the next section, the tunneling current depends exponentially on the tip–surface distance, typically varying by about an order of magnitude for a change of only 1 Å in this distance. Thus, while scanning the tip over a surface, topographic changes such as the presence of a surface step will appear as changes in the tunneling current.

(1) For reviews see: Williams, R. H.; McGovern, I. T. In *The Chemical Physics of Solid Surfaces and Heterogeneous Catalysis*, King, D., Woodruff, D. P., Eds.; Elsevier: New York, 1984; Vol. 3. Joyce, B. A.; Foxon, C. T. In *Simple Processes at the Gas-Solid Interface, Comprehensive Chemical Kinetics*; Bamford, F. H., Tipper, C. F. H., and Compton, R. G., Eds.; Elsevier: New York, 1984; Vol. 19. Haneman, D. *Rep. Prog. Phys.* 1987, 50, 1045.

(2) See for example: Woodruff, D. P.; Delchav, T. A. *Modern Techniques of Surface Science*; Cambridge University Press: Cambridge, UK., 1988.

(3) Binnig, G.; Rohrer, H.; Gerber, Ch.; Weibel, E. *Phys. Rev. Lett.* 1982, 49, 57.

(4) For reviews see: Binnig, G.; Rohrer, H. *Rev. Mod. Phys.* 1977, 57, 615. Hansma, P. K.; Tersoff, J. *J. Appl. Phys.* 1987, 61, R1. Hansma, P. K.; Elings, V. B.; Marti, O.; Bracker, C. E. *Science* 1988, 242, 157. Hamers, R. *Annu. Rev. Phys. Chem.* 1989, 40, 531.

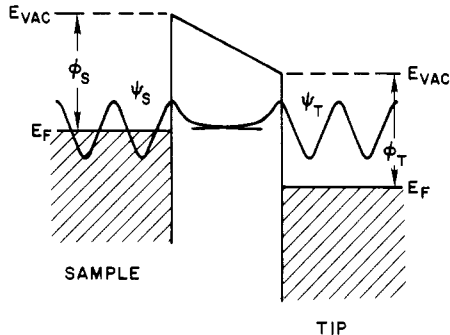


**Figure 1.** Schematic energy level diagram illustrating the overlap of the exponentially decaying wave functions of the sample and tip in the vacuum barrier region. The sample is biased negative and the tunneling involves the flow of electrons from the occupied states of the sample to the unoccupied states of the tip.

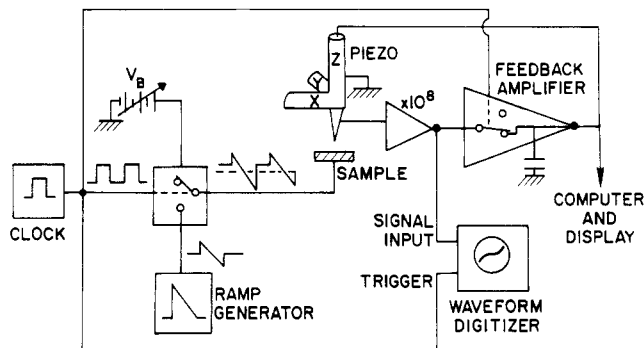


**Figure 2.** Schematic diagram of the experimental setup. Constant-current topographs are obtained with a dc bias applied to the sample and an active feedback loop. The spatial variation of the voltage applied to the z piezo so as to maintain a constant current defines the topograph. To obtain spectra ( $I$ - $V$  curves) along with a topograph, a clock and a ramp generator are used to produce a waveform consisting of a dc part and a ramp. During the dc part, topographic information is obtained, while during the ramp the feedback loop is inactive so that the tunneling current can be measured as a function of applied voltage.

Actually, however, one performs the scan keeping the tunneling current constant. This is accomplished by the use of a feedback loop (see Figure 2) which maintains a predetermined, constant tunneling current. By applying a voltage on the z piezo the tip-surface distance is changed so as to maintain this constant current. The STM topographs shown in this article are maps of the voltage applied to the z piezo-translator so that a constant current of, typically, 1 nA, is maintained.

As we will discuss in some detail in section IV, the STM can also be used to obtain tunneling spectra with atomic resolution. In our experiments,<sup>5</sup> instead of applying a dc bias to the sample, a waveform composed of a dc part and a voltage ramp generated by a clock and a ramp generator is applied to the sample (see Figure 2). During the dc part the feedback loop is active and thus a constant-current topograph of the sample is obtained. When the ramp is applied, the feedback loop is inactive, the tip-surface distance is fixed, and the tunneling current is measured as a function of the sample voltage. Thus, a grid of points on the topograph is formed for which we have complete tunneling spectra. The distance between such points is preselected and is usually one to a few angstroms.

### III. Basic Concepts

Most treatments of the tunneling process in STM are based on Bardeen's tunneling-Hamiltonian formalism.<sup>6</sup> This model is valid when the tip-surface interaction is weak so that the unperturbed wave functions of the sample ( $\phi_S$ ) and the tip ( $\phi_T$ ) can be used in the calculation of the tunneling current. The current

is then obtained by using first-order perturbation theory:

$$I = \frac{2\pi e}{\hbar} \sum_{S,T} f(E_T) [1 - f(E_S + eV)] |M_{ST}|^2 \delta(E_T - E_S) \quad (1)$$

In (1),  $f(E)$  is the Fermi-Dirac distribution function which gives the probability that a state of energy  $E$  will be occupied. Thus,  $f(E_T)$  gives the probability that a tip state of energy  $E_T$  will be occupied, while  $1 - f(E_S + eV)$  gives the probability that a sample state of energy  $E_S + eV$ , where  $V$  is the applied bias, is empty. The "matrix element"  $M_{ST}$  is given by

$$M_{ST} = \frac{\hbar^2}{2m} \int dA (\psi_S^* \nabla \psi_T - \psi_T \nabla \psi_S^*) \quad (2)$$

The integral in (2) is over any surface ( $A$ ) lying entirely within the barrier region separating the tip and sample.

We can use eq 1 and 2 to illustrate some basic aspects of STM. Let us assume that tunneling takes place between two electrodes made of the same free-electron metal with a work function  $\phi$ . Moreover, we assume that the tunneling is one-dimensional. The wave functions of the tip and sample in the barrier region will be decaying exponentials, and if the tip-sample distance is  $s$ , they can be written as

$$\psi_S = \psi_S^0 e^{-kz} \quad \text{and} \quad \psi_T = \psi_T^0 e^{-k(s-z)} \quad (3)$$

In (3),  $z$  is the distance perpendicular to the surface plane, and  $k$ , the inverse decay length of the wave functions, is given by  $k = (2m\phi/\hbar^2)^{1/2}$ . For a work function of 4 eV,  $k = 1 \text{ \AA}^{-1}$ . By substituting eq 3 into (2) and the result into (1) we find that

$$I \propto \sum_{S,T} |\psi_S^0|^2 |\psi_T^0|^2 e^{-2ks} \quad (4)$$

Equation 4 shows the exponential dependence of the tunneling current on the tip-sample separation  $s$ . For a typical inverse decay length of  $k = 1 \text{ \AA}^{-1}$ , changing  $s$  by only 1 Å will change  $I$  by  $e^2$ . This strong dependence of  $I$  on  $s$  gives STM the ability to study the topography of surfaces. The quantities  $|\psi_S^0|^2$  and  $|\psi_T^0|^2$  give the state densities at the surfaces of the sample and tip, respectively. Equation 4 shows that, by keeping the tunneling current constant while scanning the tip over the surface, one can obtain information about the electronic structure ( $|\psi_S^0|^2$ ) and topography ( $s$ ) of the surface. In the above simple theoretical analysis no distinction was made between tip and sample. However, in STM studies we are interested in the properties of the sample, while the structure and states of the tip are, in general, not known. Ideally a tip should have the maximum possible resolution and measure the properties of the bare surface without any features associated with its own electronic structure. That is, an ideal STM tip would be a mathematical point source of current. In this case, and in the limit of small bias and temperature<sup>7</sup>

$$I \propto \sum_S |\psi_S(\vec{r})|^2 \delta(E_S - E_F) \\ \rho(E_F, \vec{r}) = \sum_S |\psi_S(\vec{r})|^2 \delta(E_S - E_F) \quad (5)$$

Thus, the tunneling current would be proportional to the local density of states  $\rho(E_F, \vec{r})$  of the sample at the tip position. Tersoff and Hamann<sup>7</sup> showed that the result expressed by eq 5 remains valid regardless of tip size, provided that the tip wave function can be adequately represented by an s-wave. In this case the tip position  $\vec{r}$  should be interpreted as the effective center of curvature of the tip, i.e., the origin of the s-wave which best approximates the tip wave function. Lang<sup>8</sup> has performed first-principles calculations using an atom adsorbed on a flat metal surface ("jellium") as a model for the STM tip and has found that indeed the STM image corresponds very closely to a map of  $\rho(E_F, \vec{r})$ . At higher bias the situation becomes more complex. Since metals show a weak variation of the local density of states with energy (d states do not in general contribute prominently in STM im-

(5) Avouris, Ph.; Wolkow, R. *Phys. Rev. B* 1989, 39, 5091. Wolkow, R.; Avouris, Ph. *Phys. Rev. Lett.* 1988, 60, 1049.

(6) Bardeen, J. *Phys. Rev. Lett.* 1961, 6, 57.

(7) Tersoff, J.; Hamann, D. R. *Phys. Rev. B* 1985, 31, 805.

(8) Lang, N. D. *Phys. Rev. B* 1986, 34, 5947; *Comments Condens. Matter Phys.* 1989, 14, 253.

ages<sup>9</sup>), STM topographs obtained at not too high a bias still give essentially  $\rho(E_F, \vec{r})$ . Of course, when the bias is high the potential is affected and the sample wave functions may be distorted. For semiconductors the situation is more complex but also more interesting. Semiconductors have a much more structured density-of-states spectrum and, more importantly, for positive bias one probes conduction-band states, while for negative bias valence-band states are being probed. The corresponding wave functions may be very different and may be localized in different positions of the unit cell. For example, in the case of GaAs(110) the occupied states are localized on As while the unoccupied states are localized on Ga.<sup>10</sup> In general, an STM topograph of a semiconductor surface does not directly give the positions of the surface atoms because the electronic structure is dominated by the presence of surface states (see next section). In cases such as that of the Si(111)-(7×7) surface, on which we focus here, the surface states are p<sub>z</sub>-like orbitals whose location does correspond to the positions of the surface Si atoms.

#### IV. Atom-Resolved Electronic Spectroscopy with the STM

One of the major new capabilities that STM brings to the study of surfaces and adsorbed species is the ability to determine the energies of their occupied and unoccupied electronic states with atomic resolution. Several different ways for doing such an experiment have been proposed.<sup>11</sup> The best approach is to position the tip over the particular surface feature of interest, fix the tip-surface distance, disable the feedback loop and measure the tunneling current as a function of the sample bias. The tunneling current, however, depends not only on the density of states at a particular energy,  $\rho(E, \vec{r})$ , but also on the electron transmission coefficient ( $T$ ). The potential barrier depends on the applied bias and thus  $k$  and  $T = \exp(-ks)$  become bias dependent. For example, in the WKB approximation

$$k = \left[ \frac{2m}{\hbar^2} \left( \frac{\phi_S + \phi_T}{2} + \frac{eV}{2} - E \right) \right]^{1/2}$$

where  $\phi$  are the work functions and  $V$  the applied bias voltage. In general

$$I = \int_{E_F}^{E_F+eV} \rho_S(E, \vec{r}) \rho_T(E-eV, \vec{r}) T(E, eV, \vec{r}) dE \quad (6)$$

where the effect of finite bias on the wave functions of the surface is included through the voltage dependence of the transmission coefficient. It is usually assumed<sup>12</sup> that the tip density-of-states distribution is structureless and thus does not significantly distort the spectrum of the sample. This is not always true; at times drastic distortions of the spectra by the tip are observed (see section VIII). Even, however, with the above assumption, it is not clear from eq 6 how one can extract spectroscopic information. The derivative  $dI/dV$  is also a function of  $T(E, eV, \vec{r})$  and the exponential dependence of  $T(E, eV, \vec{r})$  on  $V$  can distort the positions of the peaks in the spectrum. Stroscio et al.<sup>13</sup> have proposed a solution to this problem. They normalize  $dI/dV$  by dividing by  $I/V$ . This procedure effectively cancels out the exponential dependence of  $T(E, eV, \vec{r})$  on  $V$ . The first-principles calculations of Lang<sup>8</sup> confirm this picture. Thus, a plot of  $(dI/dV)/(I/V)$  vs  $eV$  corresponds to roughly a density-of-states spectrum on top of a usually smoothly varying background.

#### V. Surface States and Reconstruction

When a solid is terminated, the surfaces created have dangling bonds. Thus, for example, the Si(111) and Si(110) surfaces have one dangling bond per surface atom, while the Si(100) surface has two dangling bonds per surface atom. Since the dangling-bond

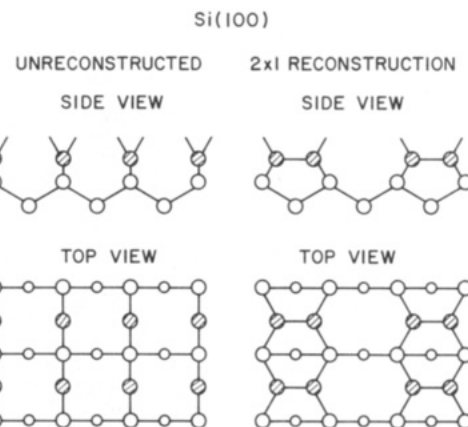


**Figure 3.** The arrangement of surface atoms (hatched) and dangling bonds at the unreconstructed Si(100) surface and at the  $2 \times 1$  symmetric dimer reconstruction.

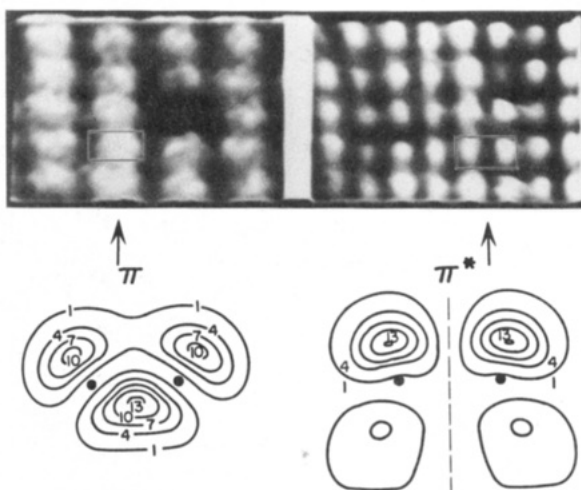


**Figure 4.** Top: Constant current topographs of (A, left) the occupied  $\pi$ -states (sample bias,  $-2$  V) and (B, right) unoccupied  $\pi^*$ -states (sample bias,  $+1.2$  V) of Si(100)-(2×1). A  $\pi$ -dimer bond and a  $\pi^*$ -antibond are enclosed in frames. A missing dimer defect can also be seen. Bottom: Charge-density contours of the  $\pi$  and  $\pi^*$ -states adapted from ref 15.

electrons are nonbonding, their energies lie in the energy gap between the valence and conduction bands of the solid. The dangling-bond-bearing surfaces produced by the ideal termination of the bulk solid have high free energy. In an effort to reduce this free energy, the surface reconstructs. Surface reconstruction may involve structural rearrangements and rebonding in the surface layer, but it may also induce changes in the bonding of subsurface layers. A good example is provided by the Si(100) surface. In the bulk-terminated (unreconstructed) surface, each surface Si atom has two dangling bonds as is shown in Figure 3. Early, low-energy electron-diffraction (LEED) studies<sup>14</sup> revealed the presence of a  $2 \times 1$  reconstruction. It is now generally accepted that this reconstruction involves alternate rows of surface atoms moving toward each other to form rows of silicon dimers as illustrated in Figure 3 (right). This dimerization process eliminates half of the surface dangling bonds. However, each of the dimer atoms still has one dangling bond. Theoretical calculations<sup>15</sup> suggested that these dangling bonds at the ends of the dimers interact weakly and form  $\pi$ -bonding and  $\pi^*$ -antibonding states. The two remaining electrons occupy the  $\pi$ -level. Thus, a weak and reactive Si  $\pi$ -bond is formed. Other calculations have suggested that the Si dimers are asymmetric: one Si atom of the dimer moves up while the other moves down. Simultaneously, there is a charge transfer from the lower atom to the higher lying

(9) Lang, N. D. *Phys. Rev. Lett.* **1987**, *58*, 45.

(10) Feenstra, R. M.; Stroscio, J. A.; Tersoff, J.; Fein, A. P. *Phys. Rev. Lett.* **1987**, *58*, 1192.

(11) Hamers, R. *Annu. Rev. Phys. Chem.* **1989**, *40*, 531.

(12) Selloni, A.; Carnevali, P.; Tosatti, P. E.; Chen, C. D. *Phys. Rev. B* **1986**, *33*, 5770.

(13) Stroscio, J. A.; Feenstra, R. M.; Fein, A. P. *Phys. Rev. Lett.* **1986**, *57*, 2579.

(14) Schlier, R. E.; Farnsworth, H. F. *J. Chem. Phys.* **1959**, *30*, 917.

(15) Appelbaum, J. A.; Baraff, G.; Hamann, D. R.; Hagstrom, H. D.; Sakurai, T. *Surf. Sci.* **1978**, *70*, 654.

one. The results of a variety of other studies favor symmetric or asymmetric dimers. In any case, the energy difference between these structures is small, so that both kinds of structures can exist at room temperature. Indeed, STM studies of this surface<sup>16</sup> showed that symmetric and asymmetric dimers coexist, with the symmetric dimers being the majority species while asymmetric dimers seem to concentrate near defect sites. In Figure 4 (top) we show topographs of (A) the occupied states of symmetric dimers (sample bias, -2 V) and of (B) the corresponding unoccupied states (sample bias, +1.2 V) from ref 17. Dimer units are enclosed in frames. Comparison with calculated<sup>15</sup> charge-density plots (Figure 4, bottom) shows clearly that STM can image the Si-Si  $\pi$ -bonds (Figure 4A) and the corresponding  $\pi^*$ -antibonding orbitals which have a nodal plane bisecting the dimer bond (Figure 4B). In more recent studies, STM has been used to image the molecular orbitals of molecules adsorbed on metals<sup>18</sup> and of a conducting organic crystal.<sup>19</sup>

## VI. Surface Chemistry Atom by Atom

We now turn to the study of surface reactions with atomic resolution. We have used two general procedures for following the spatial distribution of surface reactions on semiconductors. In the simplest case, the sample bias is adjusted so as to image the dangling-bond sites of the surface. When reaction occurs at such a site, the initially nonbonding dangling-bond electrons become involved in chemical bonds and occupy high binding energy bonding states. Corresponding antibonding states are also formed. Thus, in topographs obtained at a bias appropriate for imaging dangling bonds, reacted sites will appear "dark" because of their vanishing contribution to the local density of states. In favorable situations a higher negative or positive sample bias can be applied so as to image the new bonding or antibonding levels. Since the tunneling current depends on both electronic structure and topography, and because reaction products lie above the plane of the clean surface, even a small overlap of tip states with the product states may produce sufficient contrast to allow their imaging. As we will see below, certain dangling-bond sites may not be easily imaged in constant-current topographs. In such a case, we have used the spectroscopic characteristics of these sites to follow their reactivity. Spectroscopic maps of large areas of the surface are obtained simultaneously with topographs as described in section VI B, and the presence or absence of a dangling-bond surface state at a particular site shows if reaction has taken place.

In the following, we will discuss some of the ways in which STM can be used in surface chemistry and the kinds of information that can be obtained, using specific examples from our own work on semiconductor surfaces. The STM is also being applied recently to study chemistry on metal surfaces. Chua et al.<sup>20</sup> have studied the initial stages of the oxidation of Cu(110), while Gritch et al.<sup>21</sup> have studied the CO-chemisorption-induced 1 × 2 to 1 × 1 structural transformation of Pt(110). As prototypes, for our discussion here, we will use reactions involving the Si(111)-(7×7) surface. The 7 × 7 reconstruction of Si(111) is one of the most complex reconstructions encountered so far in surface science. Since its first observation,<sup>22</sup> it has been the subject of intense experimental and theoretical studies. Currently, the reconstruction model proposed by Takayanagi et al.<sup>23</sup> is generally accepted. The first STM studies of the 7 × 7 surface by Binning et al. played an important role in the elucidation of its structure. The Ta-

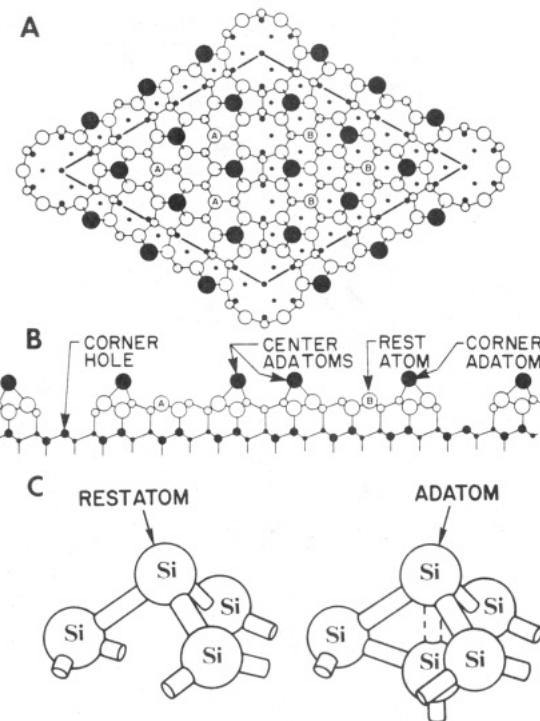


**Figure 5.** (A) Top view of the dimer-adatom-stacking fault model of the Si(111)-(7×7) reconstruction by Takayanagi et al.<sup>23</sup> The 7 × 7 unit cell containing the stacking fault (left side) is outlined. Atoms at increasing distances from the surface are indicated by circles of decreasing size. The large solid circles denote the 12 adatoms. The circles labeled A and B represent the restatoms in the faulted and unfaulted halves, respectively. Small open circles along the boundary of the unit cell represent the Si atoms forming the dimers. (B) Side view along the long diagonal of the unit cell. (C) Local structure and bonding at restatom and adatom sites.

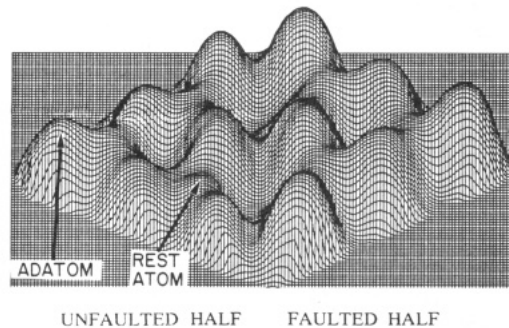


**Figure 6.** Three-dimensional STM topograph of the occupied states of the Si(111)-(7×7) unit cell (sample bias, -3 V).

kayanagi model is illustrated in Figure 5, which shows a top view and a side view along the long axis of the unit cell. In this picture, atoms at increasing depth from the surface are represented by circles of decreasing diameter. There are two triangular subunits surrounded by Si dimers. These subunits are rendered inequivalent by a stacking fault in the left subunit which helps to eliminate surface dangling bonds. A large reduction in the number of surface dangling bonds occurs when Si atoms ejected from the original surface become adatoms on top of what is now the second atomic layer, each one of them eliminating three dangling bonds on that layer while introducing a new one. Finally, at the corners of the unit cell there are Si vacancies. As a result of this reconstruction, from the 49 original dangling bonds only 19 survive in the 7 × 7 unit cell. Six of them are located on the now second layer, triply coordinated Si atoms (A and B in Figure 5)—the so-called rest atoms. Twelve are on the adatoms, and finally one dangling bond is located at the atom on the bottom of the corner vacancy, the so-called corner hole. For reasons that will become apparent later in the discussion, we further separate the adatoms in two groups: the six located near to a corner hole are called

(16) Tromp, R. M.; Hamers, R. J.; Demuth, J. E. *Phys. Rev. Lett.* **1985**, 55, 1303.

(17) Hamers, R. J.; Avouris, Ph.; Bozso, F. *Phys. Rev. Lett.* **1987**, 59, 2071.

(18) Ohtani, H.; Wilson, R. J.; Chiang, S.; Mate, C. M. *Phys. Rev. Lett.* **1988**, 60, 2398.

(19) Sletor, T.; Tycko, R. *Phys. Rev. Lett.* **1988**, 60, 1418.

(20) Chua, F. M.; Kuk, Y.; Silverman, P. J. *Phys. Rev. Lett.* **1989**, 63, 386.

(21) Gritch, T.; Coulman, D.; Behm, R. J.; Ertl, G. *Phys. Rev. Lett.* **1989**, 63, 1086.

(22) Schlier, R. E.; Farnsworth, H. E. *J. Chem. Phys.* **1959**, 30, 120.

(23) Takayanagi, K.; Nanishiro, Y.; Takahashi, M.; Motoyoshi, H.; Yagi, K. *J. Vac. Sci. Technol. A* **1985**, 3, 1502.

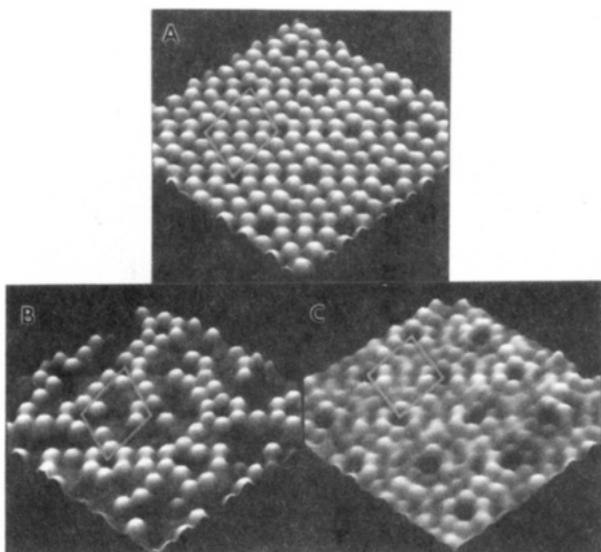


**Figure 7.** (A) STM topograph of the unoccupied states of the clean Si(111)-(7×7) surface (sample bias, +0.8 V). A unit cell with its 12 adatoms is outlined. (B) Topograph obtained after (A) was exposed to NH<sub>3</sub> (bias, +0.8 V). Reacted adatoms appear dark. (C) The same surface as in (B) imaged with a sample bias of +3 V. Both reacted and unreacted adatoms sites are visible. The 7 × 7 reconstruction is preserved overall by the reaction.

corner adatoms while the six not neighboring corner holes are called center adatoms. In Figure 6, I show an STM topograph of the occupied states of the 7 × 7 unit cell obtained with the sample biased at -3 V.<sup>5</sup> The two triangular subunits showing the presence of the stacking fault, the adatoms, and rest atoms are all clearly evident. We also note that the adatoms are more prominent on the faulted half of the unit cell, while the rest atoms are more prominent on the unfaulted half. It is clear that the 7 × 7 surface is ideal for STM studies of atom-resolved chemistry because of the presence of several different dangling-bond sites which allow one to study the role of the local environment on the reactivity of dangling bonds.

**Site-Specific Reaction of NH<sub>3</sub> with Si(111)-(7×7).** (A) *To-* *topographs.* Our first example of atom-resolved chemistry involves the reaction of Si(111)-(7×7) with NH<sub>3</sub>.<sup>5</sup> Studies of this reaction using vibrational spectroscopy<sup>24</sup> and photoelectron (photoemission, in the physics literature) spectroscopy<sup>25,26</sup> have shown that at room or even lower temperatures NH<sub>3</sub> dissociates on the 7 × 7 surface producing surface Si-H and Si-NH<sub>2</sub> groups. In Figure 7A we show an STM topograph of the unoccupied states of the clean surface (sample bias, +0.8 V); the 7 × 7 unit cell is outlined. Under these conditions the 12 adatoms in the 7 × 7 unit cell are imaged. If now we expose the 7 × 7 surface to about 2 langmuirs of NH<sub>3</sub> (1 langmuir = 1 × 10<sup>-6</sup> Torr·s), reaction takes place and with the same +0.8 V bias we obtain the topograph shown in Figure 7B. We see that roughly half of the adatom sites appear unchanged, while the other half of the sites appear dark. Following our reasoning in the previous section, the dark adatoms should be the ones that have reacted with NH<sub>3</sub> and thus lack a dangling bond. This is verified by exposing the surface to more NH<sub>3</sub>, which leads to more adatom sites turning dark. From topograph 7B it is clear then that indeed we can directly observe the spatial distribution of the reaction among the adatoms on an atom-by-atom basis. Even from a simple inspection of a topograph such as Figure 7B, important chemical information can be obtained. For example, we observe that there are roughly 4 times as many unreacted corner adatoms than center adatoms. The fact that center adatoms are more reactive than corner adatoms would be difficult, if indeed possible, to determine by conventional surface science techniques.

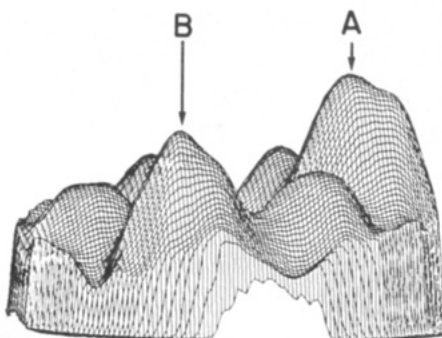


**Figure 8.** Three-dimensional STM topograph of a group of six adatom sites surrounding a corner hole. Sites A and B are reaction products while the remaining sites are unreacted.

Next we increase the sample bias to +3 V. At this energy there is a finite contribution to the local local density-of-states by reaction product states. As a result, product sites can be imaged. Figure 7C shows both unreacted adatoms and the reaction products. We can directly observe that the reaction with NH<sub>3</sub> preserves the 7 × 7 reconstruction. The reaction products are even better imaged in the occupied states mode. In Figure 8 we show a three-dimensional topograph of the occupied states of six adatom sites surrounding a corner hole (sample bias, -3 V). The strong features A and B are images of the reaction products, while the remaining features are images of the four unreacted adatoms. Imaging of reaction products is feasible because of both electronic and topographic effects. The high intensity of product-related features reflects an increased contribution from the density of states of reaction products at this energy, plus the fact that these products lie at some height above the plane of the clean surface. Another interesting feature of such topographs is the fact that these product sites appear to come in two "sizes" (size of A larger than that of C). The exact chemical nature of the species images at these sites cannot be directly deduced from the topographs. However, electron energy loss<sup>24</sup> and photoelectron<sup>25,26</sup> spectroscopic studies have confirmed the presence of Si-NH<sub>2</sub> and Si-H surface species after reaction of Si(111)-(7×7) with NH<sub>3</sub>. It is tempting then to assign the two types of product features to surface Si-NH<sub>2</sub> and Si-H groups. If this is true, then on the basis of their relative contributions to the local density of states at the particular tunneling energy (as judged from the photoelectron spectra), and their physical size, the larger features should correspond to the Si-NH<sub>2</sub> species and the smaller ones to Si-H species. We will return to this point in section VIC.

In order to answer questions such as the chemical identity of the products we need a technique with the ability to fingerprint molecular structure, such as vibrational spectroscopy. In principle, it should be feasible to measure vibrationally inelastic tunneling with atomic resolution with the STM, and some preliminary results have already been reported.<sup>27</sup> The capability of obtaining vibrational spectra with atomic resolution will certainly greatly enhance the power of STM in chemistry. However, while vibrational spectroscopy with the STM still poses technical problems, atom-resolved electronic spectroscopy with the STM is already practiced successfully by several groups and can provide unique information about local electronic structure and its relation to reactivity.

(B) *Atom-Resolved Tunneling Spectroscopy.* Using the experimental set up described in section II, we can study the electronic spectra of the clean and NH<sub>3</sub>-exposed Si(111)-(7×7) with atomic resolution. In Figure 9a we show spectra of the clean surface. Spectrum A is obtained over a rest-atom site, spectrum B over a corner-adatom site, and spectrum C over a center-adatom site. In Figure 9 negative energies correspond to occupied states, while positive energies correspond to unoccupied states. The rest-atom spectrum (A) shows a strong occupied states peak at about 0.8 eV below E<sub>F</sub>. This peak is characteristic of the rest-atom

(24) Tanaka, S.; Onchi, M.; Nishijima, M. *Surf. Sci.* 1987, 191 L756.

(25) Kubler, L.; Hill, E. K.; Bolmont, D.; Gewinner, G. *Surf. Sci.* 1987, 183, 503.

(26) Bozso, F.; Avouris, Ph. *Phys. Rev. B* 1988, 38, 3943.

(27) Smith, D. P.; Kirk, D. M.; Quate, C. F. *J. Chem. Phys.* 1987, 86, 6034.

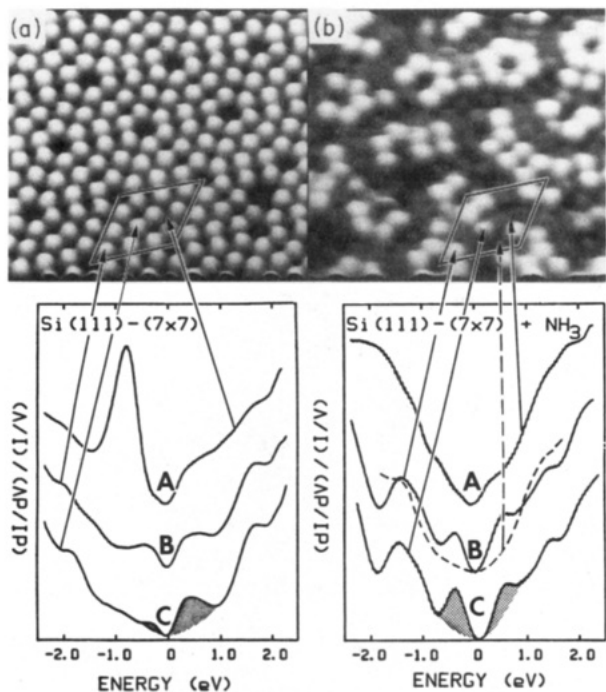


**Figure 9.** (a) Topograph of the unoccupied states of the clean  $7 \times 7$  surface (top) and atom-resolved tunneling spectra (below). Curves A, B, and C give the spectra over rest-atom, corner-adatom, and center-adatom sites, respectively. (b) Topograph of the unoccupied states (top) and atom-resolved tunneling spectra (below) of an  $\text{NH}_3$ -exposed surface. Curve A gives the spectrum over a reacted restatom site, curve B (dashed) gives the spectrum over a reacted corner adatom, while curves B (solid line) and C give the spectra over unreacted corner and center adatoms, respectively.

dangling bond. The corresponding dangling-bond states of the adatoms appear near 0.5 eV (B and C). The energies of all these surface states are in very good agreement with the results of conventional, i.e., surface area-averaged photoemission (occupied states), and inverse-photoemission (unoccupied states) spectroscopies.<sup>28</sup> The magnitude of the electron-electron Coulomb repulsion is suggested by a variety of studies to be about 0.4 eV.<sup>29</sup> Thus, the high binding energy (-0.8 eV) rest-atom dangling-bond state should be fully occupied. Theoretical studies by Northrup<sup>29</sup> have suggested that there should be charge transfer from the adatom sites to rest-atom sites. This conclusion is supported by the fact that we find reproducibly the occupied center-adatom dangling-bond state (C) to be weaker than the corner-adatom state (B). In the Takayanagi<sup>23</sup> model of the  $7 \times 7$  surface, center adatoms have two rest-atom neighbors, while corner adatoms have only one. Thus, a larger charge transfer from center adatoms can be explained in terms of local structure. As we discussed in section IV, the intensities of  $(dI/dV)/(I/V)$  vs  $eV$  spectra are not strictly proportional to the corresponding densities of states. However, computer simulations<sup>30</sup> show that the density of states of high binding energy occupied levels is underestimated in  $(dI/dV)/(I/V)$  vs  $eV$  plots, so the strong observed intensity of the higher binding energy rest-atom dangling-bond state as compared to the adatom dangling-bond states should reflect differences in the occupation and/or nature of these states. Finally, we point out the weak features at about -2 eV present in the adatom spectra B and C. Electronic structure calculations,<sup>29,31</sup> assign these features to surface resonances with adatom back-bonding character.

In Figure 9b (right) we show spectra obtained after the  $7 \times 7$  surface has been exposed to a few langmuirs of  $\text{NH}_3$  and roughly half of the adatom dangling bonds have been eliminated. If we probe the rest-atom sites on this surface, we do not find any of

them having the characteristic dangling-bond state at -0.8 eV. Instead, a structureless spectrum such as that shown in curve A is observed. More systematic studies involve spectral maps of large areas of the partially reacted surface. In these maps, spectra are obtained at prefixed intervals (e.g., every few angstroms) along with a constant-current topograph. In this way, a grid of points for which tunneling spectra have been obtained can be overlaid on the topograph, and the state (reacted or unreacted) of a particular dangling-bond site can be determined. This is another way by which the spatial distribution of a surface reaction can be observed. This approach is especially valuable when particular sites, the second-layer rest-atom sites in this case, are not easily imaged in constant-current topographs. Using such spectral maps we found that rest atoms are more reactive than adatoms, reacting faster than one would predict on the basis of their relative numbers on the  $7 \times 7$  surface. We also confirmed that center adatoms are more reactive than corner adatoms.

Spectra B and C of unreacted corner and center adatoms on the partially reacted surface (Figure 9b, right) illustrate the effects of the reaction on the electronic structure of still unreacted sites. Curves B, C (Figure 9b) show that, after the neighboring rest atoms have reacted, the electronic spectra of unreacted corner and center adatoms become virtually indistinguishable. The differences between the two sets of adatom spectra can be explained in terms of the effect of the reaction on the charge-transfer interactions present on the clean  $7 \times 7$  surface.<sup>5</sup>

Figure 6 showed a clear asymmetry between the two halves of the  $7 \times 7$  unit cell. In fact the asymmetry was found to persist even after the adatom layer was removed by chlorine etching.<sup>32</sup> This asymmetry reflects the presence of a stacking fault in the right half of the unit cell (see Figure 5A). While the normal stacking of atomic layers follows the sequence (bCcA)aB, the faulted half has the sequence (bCcA)a/C, where the slant indicates the stacking fault. The energy difference between the two configurations in Si(111)-(1×1) is very small. The stacking fault, however, plays an important role in the  $7 \times 7$  reconstruction because it leads to a reduction of the dangling-bond density. The question arises: has the stacking fault, being a subsurface feature, any effect on surface chemistry? In the case of the  $\text{NH}_3$  reaction we have not observed a significant difference. However, interesting effects were reported to occur during the early stages of nucleation of metals such as Pd,<sup>33</sup> Ag,<sup>34</sup> and Li<sup>35</sup> evaporated on Si(111)-(7×7). In all cases it was found that the faulted half was preferred and the metal atoms appeared to bond to rest atoms and center adatoms.

From the examples presented in this section, it is clear that STM topographs at different energies and atom-resolved tunneling spectra allow one to directly visualize the spatial distribution of a surface reaction and determine reactivity and electronic structure with atomic resolution.

(C) *The Reaction between Surface Structure and Reactivity.* Although the main purpose of this article is to illustrate some of the ways STM can be used to obtain chemical information, it is important to consider how local structure may be reflected in the chemical reactivity of the various dangling bond sites of the  $7 \times 7$  surface. In the Takayanagi model<sup>23</sup> of the  $7 \times 7$  reconstruction (Figure 5), rest-atom sites involve triply coordinated surface Si atoms. Calculations<sup>36</sup> find a normal dangling-bond character at these sites and a dihedral angle between bonds close to tetrahedral. Reaction at these sites should not produce surface strain. The situation is different at adatom sites. Both theory<sup>36,37</sup> and experiment<sup>38</sup> agree that adatom sites involve considerable strain. Adatoms in the Takayanagi model are members of three four-

(28) Himpel, F. J.; Fauster, Th. *J. Vac. Technol. A* **1984**, 2, 815.

(29) Northrup, J. E. *Phys. Rev. Lett.* **1986**, 57, 154.

(30) Lyo, I. W.; Avouris, Ph. Unpublished work.

(31) Qian, G.-X.; Chadi, D. J. *J. Vac. Sci. Technol. A* **1987**, 5, 906.

(32) Villarrubia, J. S.; Boland, J. J. *Phys. Rev. Lett.* **1989**, 63, 306.

(33) Koehler, U. K.; Demuth, J. E.; Hamers, R. J. *Phys. Rev. Lett.* **1988**, 60, 2499.

(34) Tosch, St.; Neddermeyer, H. *Phys. Rev. Lett.* **1988**, 61, 349.

(35) Hashizume, T. *Proceedings of STM '89*. To be published.

(36) Qian, G.-X.; Chadi, D. J. *Phys. Rev. B* **1987**, 35, 1288.

(37) Vanderbilt, D. *Phys. Rev. Lett.* **1987**, 59, 1456. Meade, R. D.; Vanderbilt, D. *Phys. Rev. Lett.* **1989**, 63, 1404.

(38) Robinson, I. K.; Waskiewicz, W. K.; Fuoss, P. H.; Norton, L. J. *Phys. Rev. B* **1988**, 37, 4325.

membered Si rings. These ring structures bring the adatoms close to the Si atoms directly below them in the third atomic layer (see Figure 5c). This proximity leads to repulsion, and distortion of the structure with adatom dihedral bond angles close to 90°. In order to reduce the strain a partial bond is formed between the adatom and the Si atom below it,<sup>5,39</sup> as indicated by dotted lines in Figure 5C. The large deviation from tetrahedral geometry and the delocalization of the dangling-bond charge at adatom sites should make these sites less favored in reactions which lead to dangling-bond saturation through a covalent bond. Another important difference between the two kinds of sites is the occupancy of the respective dangling-bond states. Atom-resolved tunneling spectra show (Figure 9a) that the rest-atom dangling-bonds are fully occupied while the adatom dangling bonds are less than half occupied. Thus, rest atoms can act as nucleophiles while adatoms can act as electrophiles. A most interesting finding is that not all adatoms react at the same rate, but that center adatoms react faster than corner adatoms. We have also observed this difference between the two kinds of adatoms in other reactions of Si(111)-(7×7) including the reaction with H<sub>2</sub>O. By reference to Figure 5 we see that there are two obvious differences between the two types of adatoms: (a) center adatoms have two rest-atom neighbors while corner adatoms have only one, and (b) corner adatoms are bonded to two Si dimers while center adatoms are bonded to only one. The first difference (a) can be important if the dissociation involves simultaneously both kinds of sites. One can envision a concerted reaction mechanism where the molecule (NH<sub>3</sub>, H<sub>2</sub>O, ...) interacts simultaneously with both sites (the adatom-restatom separation is ~4 Å) and dissociates with one fragment attached to the adatom and the other to the rest atom. The opposite charge state of adatoms and rest atoms will favor such a dissociation. Since there are twice as many rest-atom/center-adatom pairs as there are rest-atom/corner-adatom pairs, a 2:1 reactivity ratio of center to corner adatoms can be the result of this mechanism. As we saw, however, the observed reactivity ratio in the case of the NH<sub>3</sub> reaction is more than 4:1. Thus, there must be other differences between the two kinds of adatoms which influence reactivity. Calculations have shown that the strain interaction of two dimers mediated by a corner adatom is substantial, leading to a distortion of the corner-adatom site. The corner adatom is displaced upwards with the angle between back bonds more removed from tetrahedral than the corresponding angle at center-adatom sites. Recent LEED studies<sup>40</sup> provide further support. Dimer-induced strain and structural distortion of corner-adatom sites as compared to center-adatom sites or the initial differences in the occupation of the two dangling-bond states may contribute to the observed reactivity difference between corner and center adatoms.

Finally, we saw that several metals tend to preferentially bond to rest atoms and adatoms of the faulted of the unit cell. The chemical difference between the faulted and unfaulted halves of the 7×7 unit cell is most likely due to electronic interactions between dangling-bond states and subsurface sites in a manner completely analogous to that occurring at adatom sites. The local atomic arrangement at rest-atom sites in the faulted half of the unit cell is similar to that of a boat-form cyclohexane. The rest atom is directly above a Si atom in the fourth atomic layer. Calculations<sup>41</sup> show the formation of states involving a bonding 1-4 interaction between the rest-atom and this Si atom. At the unfaulted half, the local atomic arrangement at rest-atom sites is similar to that of the chair form of cyclohexane and there is no bonding 1-4 interaction.

From the above discussion, it is clear that surface chemistry is very sensitive to subtle changes in the local environment of the reacting sites. STM promises to be a powerful tool for the study of such effects. Moreover, once the atomic origin of a given surface state feature has been determined by STM and atom-resolved

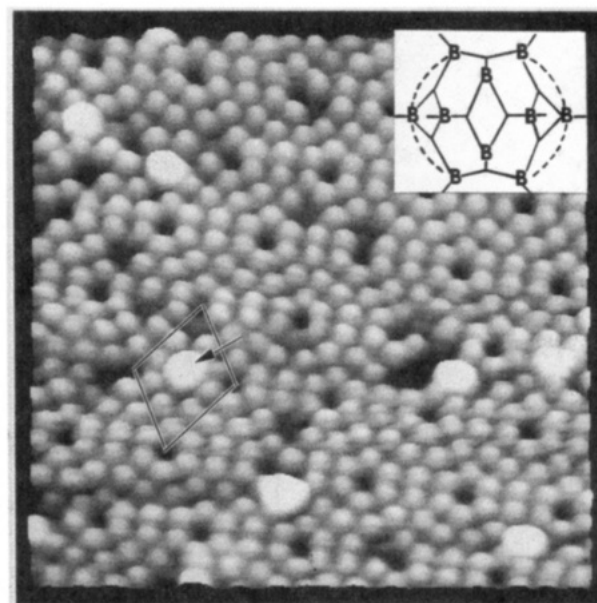


**Figure 10.** STM topograph of the Si(111)-(7×7) surface with adsorbed nido-decaborane molecules appearing as round disks. Sample bias, +2 V. The inset shows a projection of the decaborane molecule along the C<sub>2</sub> axis.

tunneling spectroscopy, then photoelectron spectroscopy can be used to quickly ascertain the gross reactivity trends for a wide range of reactants and experimental conditions. In this way we have found that, while reaction of Si(111)-(7×7) with species such as NH<sub>3</sub>, PH<sub>3</sub>,<sup>42</sup> and Si<sub>2</sub>H<sub>6</sub><sup>43</sup> favors the rest-atom sites, several reactions mainly involving open-shell systems, such as O<sub>2</sub> and NO, prefer adatom sites.<sup>44</sup> Reactions at adatom sites may not only involve the dangling bonds but also the weak and strained adatom back bonds. The strain can be relieved by breaking the back bond and attaching groups at either end, or by inserting atoms such as O so as to enlarge the size of the original four-membered Si ring.

## VII. Complex Surface Reactions

*The Interaction of B with Si-Doping Effects on Surface Reactivity.* In the previous section we discussed the reaction of Si(111)-(7×7) with NH<sub>3</sub>, which under mild conditions preserves the 7×7 reconstruction. STM can also be used to study more complex surface reactions involving much more extensive atomic rearrangements. Such is the case of the high-temperature reaction of B with Si(111)-(7×7).<sup>45</sup> This example provides the opportunity to demonstrate how STM and atom-resolved tunneling spectroscopy measurements can be coupled with first-principles calculations to provide insight into the factors that determine the nature of adsorption sites at surfaces.

As a source of B a molecular species, decaborane (nido-B<sub>10</sub>H<sub>14</sub>, DB), was used.<sup>45</sup> At room temperature DB adsorbs molecularly on Si(111)-(7×7) (the exact nature of the chemisorbed state is not known) and as Figure 10 shows, the STM can be used to directly image the DB molecules, which appear as round disks when viewed from above. As in the case of NH<sub>3</sub>, one can use such topographs to see if there are preferred adsorption sites for DB on Si(111)-(7×7). We find that again adsorption prefers center adatom sites along with defect sites. On heating the surface to temperatures above the hydrogen desorption temperature, the DB molecules dissociate and B is deposited on the surface. In Figure 11 we show a topograph of the surface after a dosing with 0.2 langmuir of DB followed by a brief heating to 600 °C. There are still large areas of the surface in the 7×7 reconstruction, but also patches with a ( $\sqrt{3} \times \sqrt{3}$ )R30° reconstruction start to

(39) Daun, W.; Ibach, H.; Muller, J. E. *Phys. Rev. Lett.* **1987**, 59, 1593.

(40) Tong, S. Y.; Huang, H.; Wei, C. M.; Pakcard, W. E.; Men, F. K.; Glander, G.; Webb, M. B. *J. Vac. Sci. Technol. A* **1988**, 6, 615.

(41) Kaxiras, E.; Avouris, Ph. Unpublished work.

(42) Avouris, Ph.; Bozso, F.; Lyo, I.-W. To be submitted for publication.

(43) Avouris, Ph.; Bozso, F. *J. Phys. Chem.*, preceding paper in this issue.

(44) Avouris, Ph.; Lyo, I. W.; Bozso, F.; Kaxiras, E. *J. Vac. Sci. Technol. A*, in press.

(45) Lyo, I.-W.; Kaxiras, E.; Avouris, Ph. *Phys. Rev. Lett.* **1989**, 63, 1261.

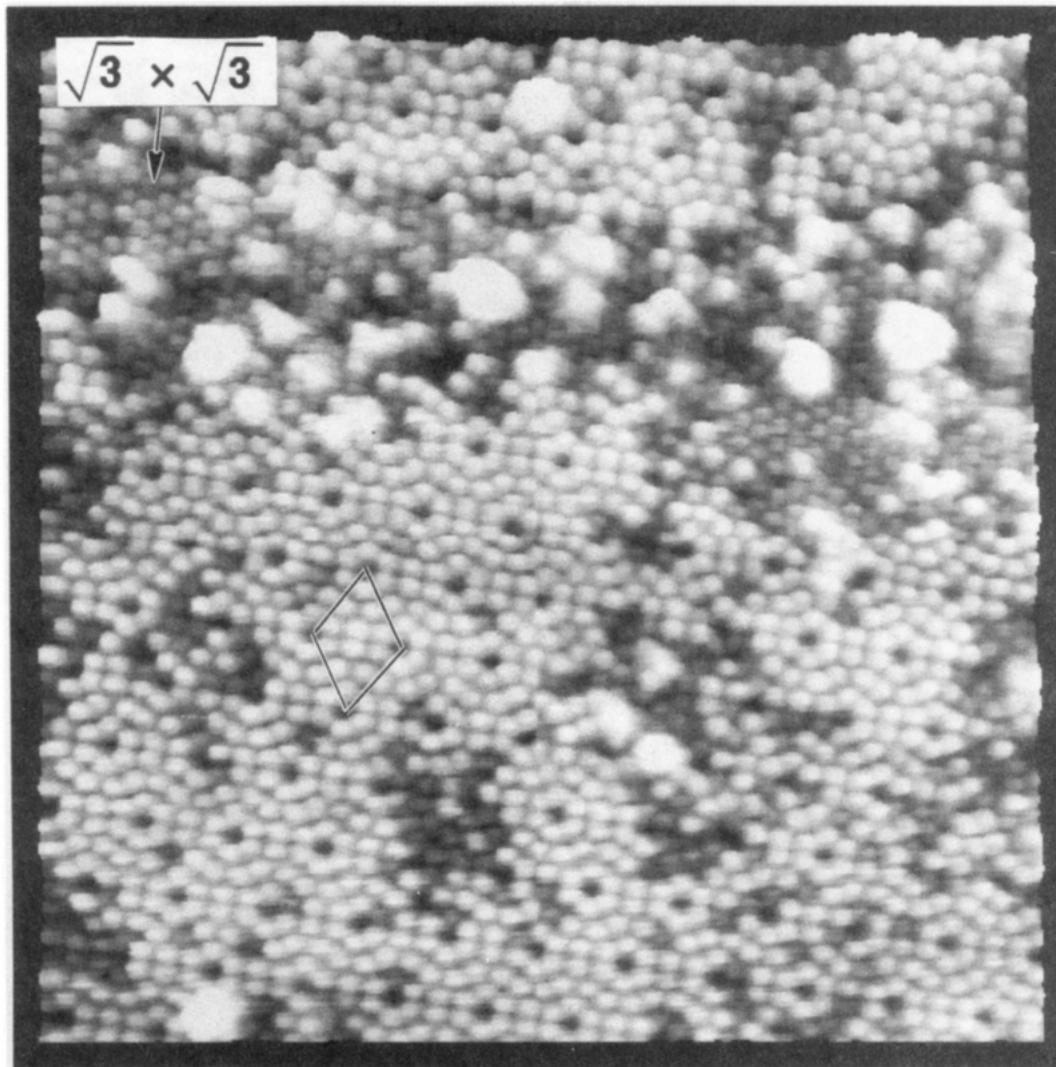


**Figure 11.** STM topograph of a Si(111)-(7×7) surface exposed to 0.2 langmuir of decaborane and briefly annealed to 600 °C.

appear. The patches are particularly prominent near the top of the picture. This is because the clean surface had a line defect in this region which acted as a trap for diffusing DB molecules and a nucleation area for the  $\sqrt{3} \times \sqrt{3}$  structure. Also observed here are globular clusters formed by displaced atoms. Further exposure to DB vapor and brief annealing to 800 °C leads to a surface such as shown in the topograph in Figure 12a. Careful observation reveals that most of the surface exhibits a  $\sqrt{3} \times \sqrt{3}$  structure. Such a structure has also been observed in LEED studies. However, it is clear that there are at least two types of sites, bright (high) and dark (low), participating in the formation of the  $\sqrt{3} \times \sqrt{3}$  surface structure.  $\sqrt{3} \times \sqrt{3}$  structures have been observed before when trivalent elements such as Al,<sup>46</sup> Ga,<sup>47</sup> or In<sup>48</sup> were adsorbed on Si(111). In all of the above cases the trivalent element was found to occupy a 3-fold site directly above a second-layer Si atom. This adatom position is usually referred to as a T<sub>4</sub> Si-adatom site (see Figure 13a). In such a site, the trivalent element can tie up three surface dangling bonds. It appears that the same situation is imaged in Figure 12a, but why two types of sites? Atom-resolved tunneling spectroscopy gives the answer: the spectra (Figure 14a) of the bright sites shown in Figure 12a are essentially identical with those of the Si adatoms on the 7 × 7 surface (see Figure 9a). Thus, the bright sites can be identified as Si adatoms in T<sub>4</sub> sites (Si-T<sub>4</sub>). The majority of the darker sites involve B atoms as adatoms at T<sub>4</sub> sites (B-T<sub>4</sub>)

(see Figure 13b). The darker appearance of these sites, as compared to the Si-T<sub>4</sub> sites, is the result of both topographic and electronic structure differences. B is smaller than Si and thus it sits about 0.4 Å lower down at the surface than Si, according to slab calculations.<sup>45</sup> In addition, the wave functions of B are more contracted than those of Si. From these results it appears that the adsorption behavior of B on Si(111) is the same as for the other group III atoms; i.e., B occupies a T<sub>4</sub>-adatom site. However, samples exposed to >1 langmuir of DB and annealed to 1000 °C form a homogeneous  $\sqrt{3} \times \sqrt{3}$  phase (Figure 12b). Using ion scattering spectroscopy<sup>49</sup> we detect only Si at this surface but the B(1s) intensity in X-ray photoelectron spectroscopy is not reduced by this treatment, indicating that B is present close to but not at the surface of the sample. The tunneling spectra of this phase shown in Figure 14b are very different from those of Si adatoms at the 7 × 7 surface. The characteristic dangling-bond states are absent and the development of a band gap is observed. First-principles electronic structure theory helps resolve the structure of this phase. Calculations<sup>45</sup> show that the Si-T<sub>4</sub> structure shown in Figure 13b is not the thermodynamically most stable configuration, but that configuration c which involves the B atom in a substitutional site with a Si adatom over it (a B-S<sub>5</sub> site) is more stable by ~1 eV. The same conclusion regarding the most stable structure of B in Si was reached independently in two other studies involving B surface segregation from heavily doped bulk Si.<sup>50,51</sup> The calculations indicate that there are two

(46) Hamers, R. J.; Demuth, J. E. *Phys. Rev. Lett.* **1988**, 60, 2527.

(47) Nicholls, J. M.; Reihl, B.; Northrup, J. E. *Phys. Rev. B* **1987**, 35, 4137.

(48) Nogami, J.; Park, S.; Quate, C. F. *Phys. Rev. B* **1987**, 36, 6221.

(49) Bozso, F.; Avouris, Ph. Unpublished work.

(50) Headrick, R. L.; Robinson, I. K.; Vlieg, E.; Feldman, L. C. *Phys. Rev. Lett.* **1989**, 63, 1253.

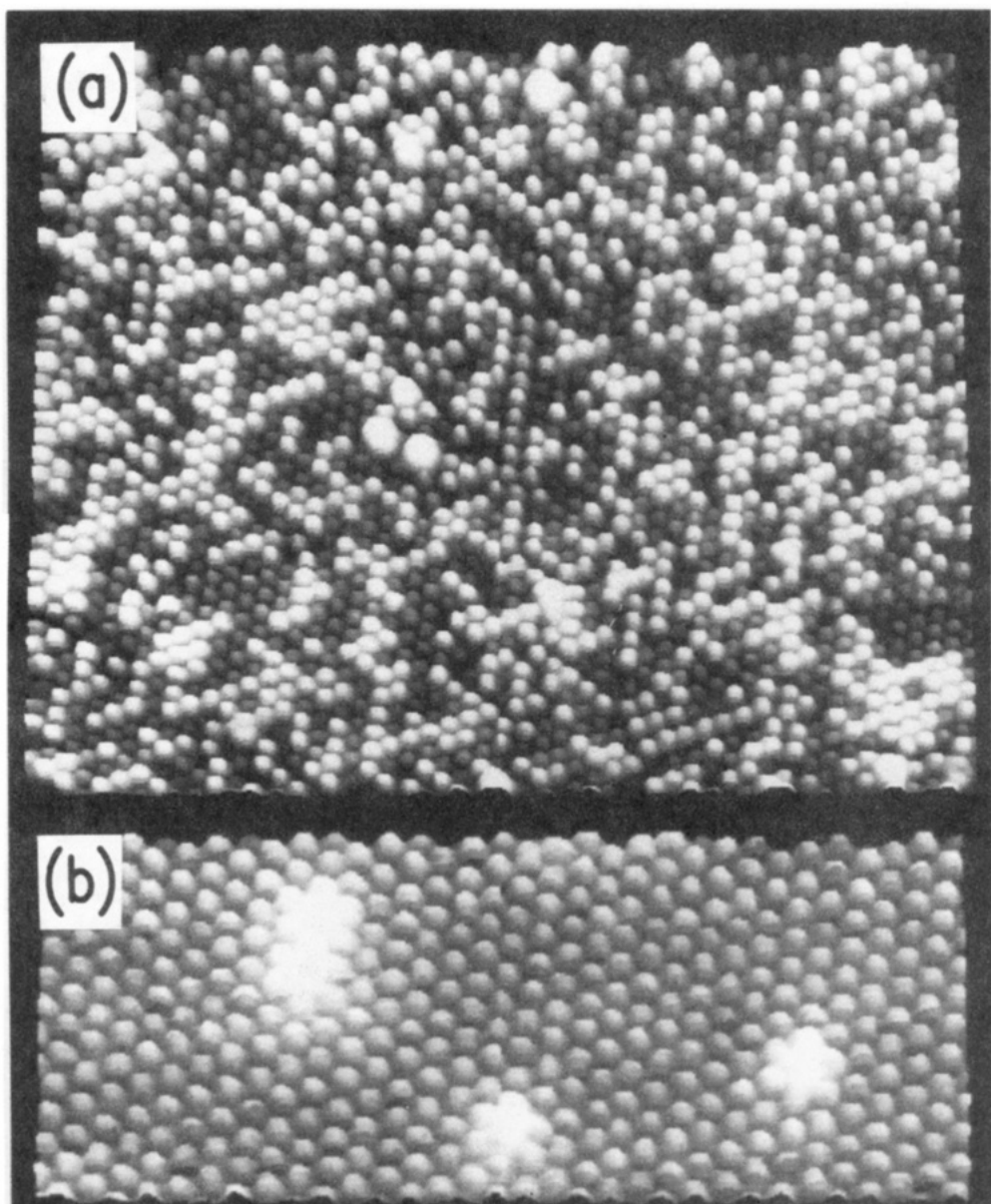


**Figure 12.** (a) STM topograph of the mostly  $\sqrt{3} \times \sqrt{3}$  surface produced by exposing the  $7 \times 7$  surface to 0.4 langmuir of decaborane and annealing briefly to 800 °C. (b) After addition of 1 langmuir of decaborane and annealing up to 1000 °C. Sample bias, +2 V.

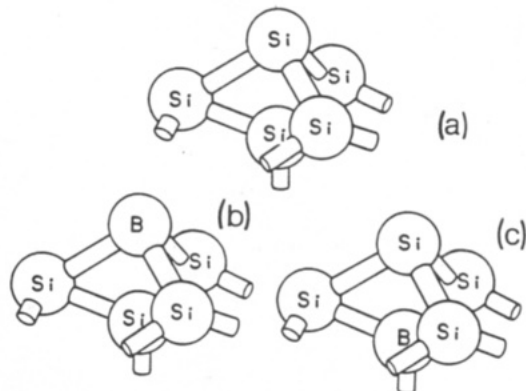


**Figure 13.** The local structures of (a) a Si-T<sub>4</sub> site, (b) a B-T<sub>4</sub> site, and (c) a B-S<sub>5</sub> site.

reasons for the stability of that configuration: (a) structure C induces much less subsurface strain than structure B and (b) by charge transfer from the Si adatom to the substitutional B atom the adatom dangling-bond state in the band gap is depopulated,

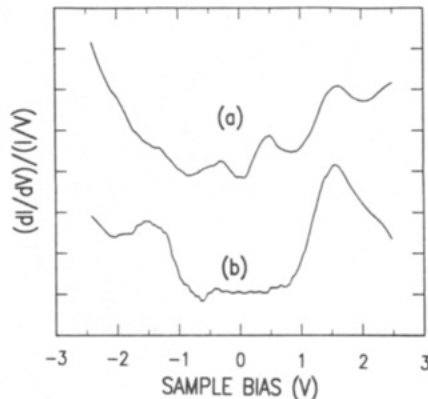


**Figure 14.** Atom-resolved tunneling spectra obtained over (a) "bright" atom sites in Figure 12a, (b) over majority sites of the  $(\sqrt{3} \times \sqrt{3})$  structure of Figure 12b.

leading to a reduction of the energy of the system. The electronic structure calculations<sup>45</sup> show that the occupied state at -1.5 eV has back-bond, not dangling-bond, character.

As we saw earlier, surface reactivity is very sensitive to the local electronic structure. Thus, the modification of the adatom

(51) Bedrossian, P.; Meade, R. D.; Mortensen, K.; Chen, D. M.; Golovchenko, J. A. *Phys. Rev. Lett.* **B** 1989, 63, 1257.

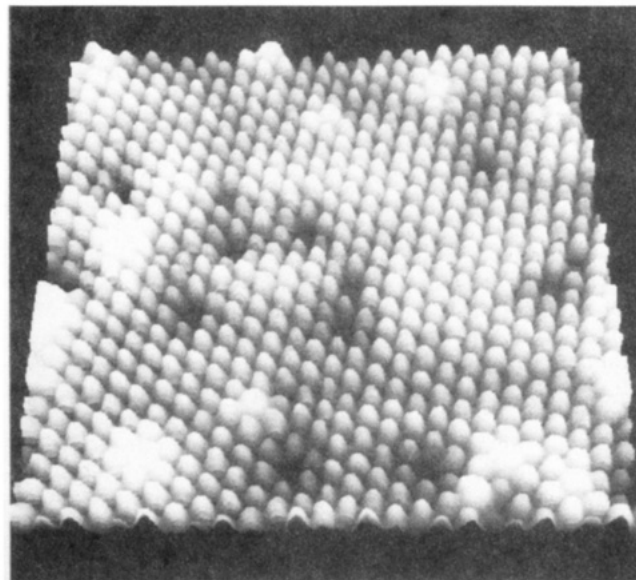


**Figure 15.** The B/Si(111)-( $\sqrt{3} \times \sqrt{3}$ ) surface after exposure to about 400 langmuirs of NH<sub>3</sub>.

electronic structure by B adsorption and the absence of rest-atom sites should be reflected in the chemical properties of the  $\sqrt{3} \times \sqrt{3}$  surface. We can test this using again NH<sub>3</sub> as a reactant. While exposure of the Si(111)-(7×7) surface to ~2 langmuirs of NH<sub>3</sub> led to the reaction of about half of all adatoms, the topograph in Figure 15 shows that even after exposure to a few hundred langmuirs of NH<sub>3</sub> hardly any reaction has taken place among Si adatoms of the B-doped surface. More interestingly, we have performed<sup>44</sup> valence photoelectron spectroscopy studies of this system at low temperatures (~100 K) which show that NH<sub>3</sub> adsorbs reversibly on the B-modified surface by donating lone-pair electrons to the empty Si dangling-bond state, that is, by a Lewis acid-base reaction. This is in contrast to the dissociative adsorption of NH<sub>3</sub> observed on the clean 7×7 surface. Thus, we see that not only the rate of a reaction but even the nature of the reaction can be changed by substrate electronic structure modification through doping. In addition to the short-range charge-transfer process discussed above, the STM results of Figure 12a suggest that there may also be a long-range effect. It is seen that the presence of B stabilizes Si-T<sub>4</sub> adatom structures. This is likely the result of the shift of the Fermi energy toward the valence band due to B-doping. This shift leads to a decrease of the energy of the  $\sqrt{3} \times \sqrt{3}$  reconstruction by depopulating the Si-T<sub>4</sub> adatom dangling-bond levels in the band gap.

### VIII. Tip Effects

The most important part of the STM is the tip which probes the structure of the sample. Yet, in general, the structure of the tip and to some extent its chemical composition are unknown. Field-emission techniques have been applied in the study of tip structure, but such studies are not routinely made. Moreover, the structure of the tip changes during an experiment as atoms and groups of atoms move on the surface of the tip. As eq 4 shows, the STM measures a convolution of the sample and tip states. However, the density of states of the tip is a function of its structure. When atomic resolution is achieved, tunneling must involve a single or at most a couple of tip atoms. It is obvious that the density of states of the bulk metal from which the tip is made should not provide a good representation of the density of states of the active area of the tip. One would expect<sup>8</sup> a peaked distribution, most probably a Lorentzian with a width that depends on the coupling of the "active area" to the rest of the tip. This coupling can be quite weak, and the corresponding density of states quite narrow, if the active region of the tip is composed of an adatom or small cluster of atoms of different chemical nature than the bulk of the tip. Foreign atoms on the tip may be present from

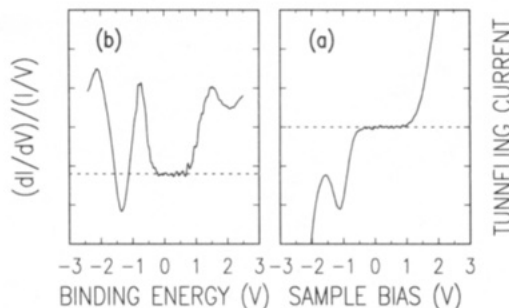


**Figure 16.** (a)  $I$ - $V$  curve of defect site showing negative differential resistance. (b) The corresponding  $(dI/dV)/(I/V)$  vs  $eV$  spectrum.

the tip preparation process (e.g., metal oxides or carbides), from exposure of the sample to reactants, or through unintentional contact of the tip with the sample surface. Tunneling spectra obtained with such tips can be distorted and show the presence of extra, tip-related features.<sup>52</sup> If the sample itself also has localized states with narrow spectral features, then such a tip-surface combination can lead to interesting  $I$ - $V$  characteristics. Such an effect can be observed in the spectra of isolated defects similar to the bright sites of Figure 12b.<sup>52</sup> The  $I$ - $V$  curve obtained over such a site (Figure 16) by a tip with a peaked density of states shows a region of negative differential resistance, i.e., a regime where the current decreases as the voltage is increased. The corresponding  $(dI/dV)/(I/V)$  plot shows a negative dip at about -1.5 eV. It is interesting to note that negative differential resistance is the key property of macroscopic electronic devices such as the Esaki diode.<sup>53</sup> The above results indicate that device-like characteristics can be obtained from surface features of atomic dimensions (about 1 nm)—an observation that may have important implications in the question of the ultimate miniaturization of electronic devices.<sup>52</sup>

Tips that give "anomalous" spectra, such as those of Figure 16, may give topographs which are indistinguishable from those obtained by using tips with unstructured density of states. We have also found many cases of tip-dependent changes in contrast between different surface features. At present, the origin of such effects is not entirely clear. They may be related to changes in the nature of the tip wave functions, which lead to differences in overlap with the charge distributions of the various surface sites.

Tip effects such as those described above do not occur very often; however, it is clear that the experimentalist should always be on the alert for them. Until better control on the tip structure is achieved, the safest approach is to repeat a given experiment several times using different tips and/or test the appearance and spectra of known structures on the sample.

### IX. The Future

In the above we discussed a few ways by which STM can be used in the study of surface chemistry. These applications in no way exhaust the possible applications of STM in chemistry. There are at least three directions in which one may expect STM applications to grow in the future:

(a) STM will be applied to many new types of materials. Currently, most applications involve metal and semiconductor surfaces in ultra-high-vacuum environments. However, there are new studies appearing on conducting organic crystals, liquid crystals, polymers, biomolecules, solid materials under liquids, and electrochemical systems. Even insulating materials may, under the appropriate conditions, be studied by the STM. This can be accomplished by nonlinear alternating-current STM,<sup>54</sup> photoexcitation of carriers to the conduction band,<sup>55</sup> or direct ejection of electrons in the conduction band.<sup>56</sup> It is already clear that

(52) Lyo, I.-W.; Avouris, Ph. *Science* **1989**, 245, 1369. Avouris, Ph.; Lyo, I.-W.; Bozso, F.; Kaxiras, E. *J. Vac. Sci. Technol. A*, in press.

(53) Esaki, L. *Phys. Rev.* **1958**, 109, 603.

(54) Kochanski, G. P. *Phys. Rev. Lett.* **1989**, 62, 2285.

(55) van de Walle, G. F. A.; van Kempen, H.; Wyder, P. *Appl. Phys. Lett.* **1987**, 50, 22.

(56) Avouris, Ph.; Wolkow, R. *Appl. Phys. Lett.* **1989**, 55, 1074.

STM is not just a surface science technique. In many studies the role of the substrate surface is analogous to that of a chemical bench on which the system of interest is placed to be studied by STM.

(b) We expect to see new types of measurements using the STM. As we discussed earlier, local vibrational spectroscopy with atomic resolution using the STM will produce an extremely powerful chemical tool. There are currently efforts in several laboratories to develop such a capability. The STM operated in the field-emission mode could be used to excite low-energy Auger transitions and, after energy analysis of the ejected Auger electrons, to determine local chemical composition. We should also expect to see time-resolved STM measurements in the future. Relatively slow surface diffusion processes can be directly imaged by using current STM technology, and fast-scanning STMs are becoming available.

(c) STM can be used not only as a probe of surface structure and chemistry, but also as an active participant. For example, one can use tunneling or field-emitted electrons from the STM tip to excite adsorbed species to dissociative states and thus induce local (nanometer scale) surface chemistry. Some promising results already exist.<sup>57</sup> In addition, reactions which are specifically induced by low-energy electrons, such as dissociative electron attachment, can be utilized. Besides the basic scientific interest in inducing nanometer-scale chemistry, the prospect of utilizing

the STM as a nanometer-scale lithographic device for applications in microelectronics is very exciting. Field-desorption and deposition of species adsorbed on the STM tip may also allow the formation of specific patterns on a surface. Finally, the STM tip itself can be used as a micromechanical device to induce morphological changes. It has already been used to "machine" surfaces,<sup>58</sup> and it is possible to dig trenches only a few atoms wide.<sup>59</sup> Perhaps, in the future, it can be used to "operate" on biomolecules.

As the applications of STM grow and it is applied under a wider range of conditions, it will be imperative that detailed studies be performed to better understand the tip–surface interaction and the nature of the STM images. The Tersoff–Hamann interpretation of the STM topographs, on which we have relied in this paper, is valid in a relatively narrow range of operating conditions. It is necessary for experimental and theoretical studies to address the issue of the nature of STM images under strong tip–surface interactions and the perturbation of the surface electronic structure by local high electric fields. In the future it may be possible to utilize the chemical specificity of strong tip–surface interactions to achieve a measure of chemical specificity in STM imaging.

**Acknowledgment.** I gratefully acknowledge my co-workers, R. Wolkow, In-Whan Lyo, R. Hamers, and F. Bozso, for their contributions to the work described in this article.

(57) McCord, M. A.; Pease, R. F. W. *J. Vac. Sci. Technol. B* 1987, 5, 430. Ehrichs, E. E.; Yoon, S.; deLozanne, A. L. *Appl. Phys. Lett.* 1988, 53, 2287.

(58) McCord, M. A.; Pease, R. F. W. *Appl. Phys. Lett.* 1987, 50, 5699.

(59) Avouris, Ph.; Wolkow, R. *Mater. Res. Soc. Symp. Proc.* 1989, 131, 157.

## ARTICLES

### Theoretical Estimation of the Maximal Value of the First, Second, and Higher Electron Affinity of Chemical Compounds

G. L. Gutsev\*

Institute of Chemical Physics of the USSR Academy of Sciences, Chernogolovka, Moscow Region 142432, USSR

and A. I. Boldyrev\*

Institute of Chemical Physics of the USSR Academy of Sciences, Moscow V-334, Kosygin str. 4, 117334, USSR (Received: December 22, 1988; In Final Form: September 20, 1989)

A method for an estimation of the maximal values of the first, second, third, and higher electron affinities (EAs) of chemical compounds is suggested. The estimation is based on the known data of energies of the highest occupied nonbonding molecular orbitals of anions. The maximal EA values for the  $MF_k$  compounds are estimated for every  $k$  from the results of quantum chemical calculations. It is found that hexafluorides may possess a second positive EA; i.e., their doubly charged anions may, in principle, be stable to the loss of an electron in an isolated state. It is shown that systems with the highest possible second and higher values of the EA should be searched among the polynuclear  $M_nX_{nk+2}$ ,  $M_nX_{nk+3}$ , etc., complexes, where  $k$  is the maximal formal valency of the M atom,  $n \geq 2$ , and X is a monovalent electronegative ligand. It is shown that the maximal EAs of chemical compounds are enclosed within a range of 10–12 eV.

The electron affinity (EA) is one of the important electronic characteristics of chemical compounds. Of special interest are the compounds with the maximal possible EAs because it is reasonable to assume that the wide range of new materials such as chemical compounds of inert gases, organic superconductors, organic metals, etc., will be synthesized on their base.

The study of the problem of systems with high EAs appears to have started with works of Bartlett.<sup>1,2</sup> He succeeded in obtaining the first compounds of inert gases using platinum hexa-

(1) Bartlett, N.; Lohmann, D. H. *Proc. Chem. Soc.* 1962, No. 1, 115.

(2) Bartlett, N.; Lohmann, D. H. *J. Chem. Soc.* 1962, No. 12, 5253.